

STP 1611, 2019 / available online at [www.astm.org](http://www.astm.org) / doi: 10.1520/STP161120180007

Aditya Ayithi<sup>1</sup> and William G. Ryan<sup>2</sup>

# Unit Side Shear in Rock-Socketed Bored Piles

## Citation

Ayithi, A. and Ryan, W. G., "Unit Side Shear in Rock-Socketed Bored Piles," *Stress Wave Theory and Testing Methods for Deep Foundations: 10th International Conference, ASTM STP1611*, P. Bullock, G. Verbeek, S. Paikowsky, and D. Tara, Eds., ASTM International, West Conshohocken, PA, 2019, pp. 97–127, <http://dx.doi.org/10.1520/STP161120180007><sup>3</sup>

## ABSTRACT

The results of 89 bidirectional axial static load tests conducted on rock-socketed bored piles are presented herein. Based on the test results, a linear empirical relation for estimating the ultimate unit side shear from rock uniaxial compressive strength is proposed. The empirical relation indicates that approximately 5 % of rock compressive strength can be used as a predesign unit side shear value. Based on a statistical analysis of the test database, multiplication factors for estimating unit side shear at different shear displacements are developed. In addition, the influences of rock strength and socket dimensions on unit side shear are evaluated. The socket embedment ratio has the greatest influence, whereas the socket diameter does not show any significant influence.

## Keywords

unit side shear, bored pile, rock socket, uniaxial compressive strength, shear displacement

## Introduction

Rock-socketed bored piles are generally designed for either socket shear resistance (i.e., frictional resistance), end-bearing resistance (i.e., tip resistance), or a combination of both. When rock socket shear resistance is considered as part of the pile

---

Manuscript received January 24, 2018; accepted for publication April 18, 2018.

<sup>1</sup>3C Drilling, LLC, 807 N West End Blvd., Quakertown, PA 18104, USA  <http://orcid.org/0000-0002-2742-6736>

<sup>2</sup>Loadtest USA, 2631-D NW 41st St., Gainesville, FL 32606, USA

<sup>3</sup>ASTM Symposium on *Stress Wave Theory and Testing Methods for Deep Foundations: 10th International Conference* on June 27–29, 2018 in San Diego, CA, USA.

design, the quantification of the unit side shear ( $f_s$ ) based on rock properties becomes very critical. The  $f_s$  of a rock socket is dependent on the frictional shear strength of the rock, rock quality, any seams and discontinuities in the rock, construction method, and roughness of the socket wall. Since the early 1970s, several researchers have proposed empirical relations for estimating the ultimate unit side shear ( $f_{s,max}$ ) from the uniaxial compressive strength ( $q_u$ ) of rock. Kulhawy, Prakoso, and Akbas [1] reviewed and discussed various empirical relations available in the literature. Some relations include the effect of rock quality designation (RQD) via a reduction factor. These empirical relations were developed primarily based on field load tests. However, it was not clear whether all the load tests that were part of the data set reached ultimate (failure) shear capacity to affirm that the developed empirical relations can estimate “true”  $f_{s,max}$ , which typically occurs at a shear displacement ( $z$ ) of 5.0 to 10.0 mm [1]. O’Neill [2] noted that the available load test data set appears to have very few load tests conducted on bored piles greater than 1,220 mm (48 in.) in diameter, a rock  $q_u > 25$  MPa, or both. With the advancement of drilling equipment and load testing technology, construction and testing of 1,220-mm and larger-diameter bored piles in stronger rock are becoming more common. Therefore, it is necessary to investigate side shear resistance of large-diameter or high  $q_u$  rock sockets, or both.

Since the advent of the bidirectional test method for deep-foundation static load testing, it has become possible to conduct full-scale load tests on large-diameter, high-capacity rock-socketed bored piles. It has been repeatedly proven that the  $f_{s,max}$  estimated from empirical formulas are much smaller than the bidirectional load test measured values [3]. In some cases, this difference was 25 times greater. Most design specifications let the engineer use an  $f_s$  value higher than the estimated value of the empirical relation if it is proven out by a full-scale load test.

In this paper, bidirectional O-cell test data for 89 full-scale load tests are presented. This data set consists of instrumented load tests conducted on bored piles with diameters varying from 560 to 2,590 mm and rock  $q_u$  varying from 5.5 to 310 MPa. For those tests in which  $f_{s,max}$  was not mobilized, a statistical analysis was performed to develop simple multiplication factors to predict  $f_s$  values at specified shear displacements ( $z$ ). Empirical relations for estimating  $f_{s,max}$  from rock  $q_u$  are developed. The influence of rock socket diameter and length on  $f_s$  is also discussed.

## Literature

The typical format of the empirical formula for estimating  $f_{s,max}$  from  $q_u$  is given in Eq 1:

$$\frac{f_{s,max}}{p_a} = B \left( \frac{q_u}{p_a} \right)^n \quad (1)$$

where:

$p_a$  = atmospheric pressure (101.325 kPa) and

$B$  and  $n$  = empirical factors derived from the load test data.

Based on their review of various empirical relations available in the literature, Kulhawy, Prakoso, and Akbas [1] concluded that an  $n$  value of 0.5 is proposed by most researchers. Based on all the reviewed test data, they also proposed a mean value of 0.98 and lower-bound value of 0.63 for  $B$ . American Association of State Highway and Transportation Officials (AASHTO) specifications [4] recommend Horvath and Kenney [5] Eq 2 after including a joint modification factor  $\alpha_E$  [6] accounting for the rock RQD, where  $f_c$  is the unconfined compressive strength of concrete. O'Neill and Reese [6] developed a table to estimate  $\alpha_E$  based on RQD and the type of joints (closed or open), and  $\alpha_E$  can be anywhere between 0.45 and 1.0. In Eq 2, it is important to note that the shear resistance of the pile-rock interface is controlled by the weaker of the two materials. AASHTO [4] states that for a 3-m-deep rock socket, approximately 12.7 mm of deformation at the top of the rock socket would mobilize  $f_{s,max}$ . Horvath and Kenney [5] reported that  $f_{s,max}$  is typically mobilized at  $z = 6$  mm.

$$\frac{f_{s,max}}{p_a} = 0.65 \alpha_E \left( \frac{\text{lessor of } (q_u \text{ or } f_c)}{p_a} \right)^{0.5} \quad (2)$$

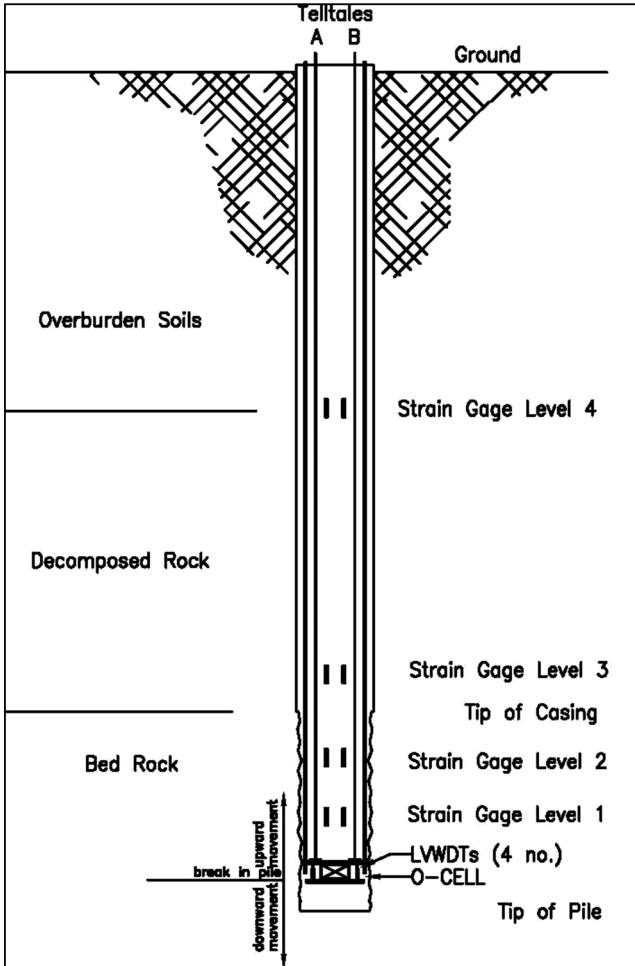
## Bidirectional Axial Load Testing and Development of Unit Side Shear Curves

Fig. 1 shows a typical schematic illustration of an instrumented bidirectional test bored pile. In a bidirectional load test, the embedded jack applies all of the axial compressive static loading within the pile and requires no external reaction system or dead load at the top of the pile. In high-capacity rock sockets, because significant reaction from end bearing can be mobilized, the hydraulic jack is typically placed at or near the bottom of the pile. In this case, the end bearing and side shear components are measured separately. A detailed description of bidirectional testing and its advantages can be found in Osterberg [7] and Ayithi et al. [8]. Bidirectional hydraulic jack expansion, pile compression, and pile displacements are measured from the installed telltales and electronic expansion gages. Vibrating wire strain gages are installed, typically at the top of each layer, to measure the strain,  $\varepsilon$ , at various depths of the pile.

The load ( $P$ ) at any given strain gage location within the pile can be calculated from the estimated pile stiffness ( $AE$ ) and measured strain gage data using Eq 3.

$$P = AE \cdot \varepsilon \quad (3)$$

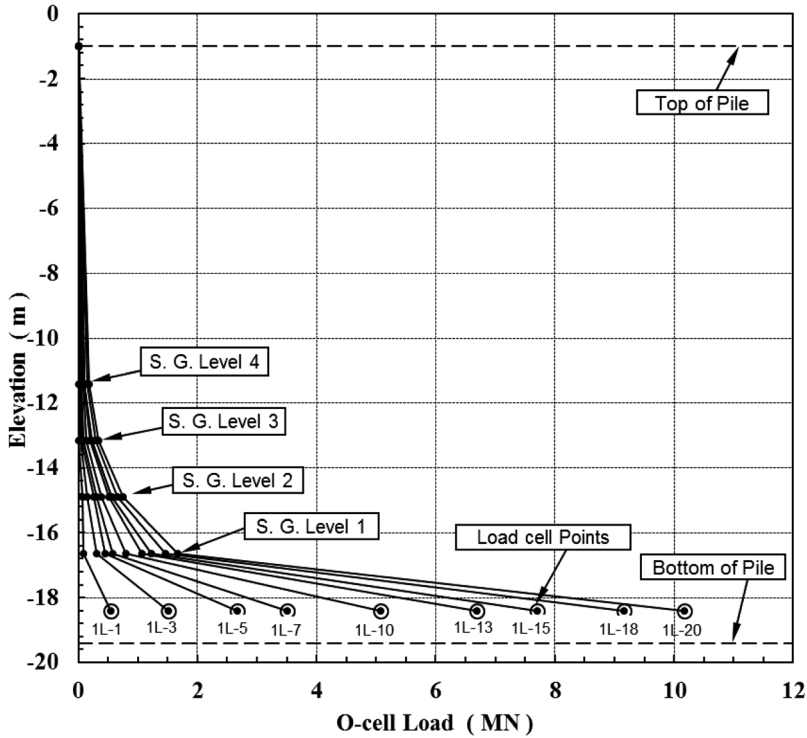
**FIG. 1** Schematic sectional view of a bidirectional test pile with embedded instrumentation.



A typical load distribution plot that can be developed from the previous calculated loads is shown in Fig. 2. From the load distribution and known side shear surface area ( $A_s$ ), the mobilized  $f_s$  for each layer can be calculated from Eq 4. Shear displacements mobilized during the test can be measured via telltales installed at required depths or estimated using  $\epsilon$  data from strain gages.

$$f_s = \frac{P}{A_s} \quad (4)$$

FIG. 2 Typical strain gage load distribution in a bidirectional load test.



## Bidirectional Load Test Data Set for Rock-Socketed Bored Piles

A summary of the results of 89 bidirectional load tests conducted on rock-socketed bored piles is presented in Table 1. Various pile and test parameters such as the type of rock and its description, rock socket diameter and length, load applied, measured  $f_s$  of the rock socket, and mobilized  $z$  are presented. Because of the bidirectional load test capabilities for applying a very high load (current record is 161.6 MN [9]), full-scale load tests on high-capacity rock-socketed bored piles can be performed successfully, possibly to failure in side shear.

The data set includes rock sockets in schist, gneiss, shale, sandstone, siltstone, claystone, limestone, calcitic marble, dolomite, diabase, granite, basalt, dolerite, and tuff rocks. Broadly categorized, the data set includes 46 sedimentary, 26 metamorphic, and 17 igneous rock formations. Rock  $q_u$  varies between 5.5 and 310 MPa, with 78 sockets (88 %) having a  $q_u \geq 25$  MPa and 33 (37 %) having a  $q_u \geq 52$  MPa. RQD varies between 20 % and 100 %; 66 sockets (67 %) have an RQD  $\geq 80$  %, and

**TABLE 1** Bidirectional load test database with rock properties, socket dimensions, and test results.

Test No.	Type of Rock	Rock Visual Description	Rock Properties			Socket Length (m)	Pile Diameter (mm)	O-Cell Applied Load (MN)	O-Cell Movements (mm)		Unit Side Shear		Concrete Strength, $f_c$ (MPa)
			$q_u$ (MPa)	RQD (%)	REC (%)				Upward	Downward	z (mm)	$f_s$ (MPa)	
1	Mica schist	Very closely jointed	33.1	83	100	4.6	914	16.5	12.2	2.5	11.9	1.9	40.8
2	Mica schist	Very closely jointed	32.4	90	95	2.7	914	5.0	5.1	2.9	5.0	1.1	37.5
3	Mica schist	Very closely jointed	32.8	91	96	4.0	1,067	24.7	4.0	2.0	4.0	2.0	75.3
4	Mica schist	Slightly to moderately fractured, closely jointed	53.1	97	100	6.3	914	26.3	12.1	4.2	11.9	7.0	90.8
5	Mica schist	Slightly to moderately fractured, closely jointed	51.7	97	100	6.8	914	25.4	5.1	8.0	5.1	6.2	95.2
6	Mica schist	Hard, fractured	59.3	90	90	4.6	864	11.1	0.9	1.4	1.4	1.1	52.7
7	Mica schist	Very hard	44.8	95	98	3.0	914	12.5	14.7	4.5	14.7	1.8	78.8
8	Mica schist	Very hard	44.1	95	98	2.4	914	13.6	15.1	2.7	14.7	4.2	82.7
9	Mica schist	Very hard	55.2	78	100	4.0	1,219	17.6	2.8	1.0	2.7	2.2	49.8
10	Mica schist	Very hard to hard	32.8	90	100	8.5	914	7.2	9.6	27.6	3.3	0.8	31.0
11	Mica schist	Very close to close, moderately hard to hard	30.3	95	100	5.5	559	3.5	0.6	2.4	0.6	0.6	44.6
12	Mica schist	Very close to close, moderately hard to hard	30.3	95	100	6.4	559	3.5	0.5	0.7	0.5	0.7	44.3
13	Mica schist	Very hard to hard	45.2	80	100	4.6	1,524	11.5	0.6	0.3	0.6	0.7	32.1
14	Mica schist	Very hard to hard	45.2	82	100	3.4	610	3.4	0.7	1.1	0.7	0.8	31.0
15	Mica schist	Very hard to hard	45.2	60	100	4.3	559	3.4	0.5	6.7	0.5	0.9	35.7
16	Mica schist	Very hard to hard	45.2	93	100	4.3	559	3.4	0.1	2.1	0.1	0.8	39.3

17	Mica schist	Very hard to hard	45.2	82	100	3.6	559	3.4	0.4	1.0	0.4	0.9	32.0
18	Gneiss	Very close to closely jointed, very hard	54.2	60	100	3.9	1,219	11.8	1.3	1.5	1.3	0.8	40.0
19	Mica gneiss	Hard, moderately spaced	112.8	82	100	2.9	762	4.0	2.4	3.1	2.3	0.7	69.1
20	Mica gneiss	Hard, moderately spaced	112.8	83	100	2.6	762	7.0	2.4	3.1	2.4	0.9	71.6
21	Gneiss	Hard, closely jointed	113.8	98	100	8.1	610	6.6	0.5	1.3	1.1	3.0	41.9
22	Gneiss	Hard, fractured	88.0	87	100	7.5	1,372	15.9	0.3	0.8	0.3	1.0	58.4
23	Gneiss	Hard, fractured	88.0	86	95	7.6	1,130	11.3	0.4	1.4	0.4	1.1	47.6
24	Schist and gneiss	Hard	55.2	100	100	3.0	965	22.0	4.1	20.6	3.8	3.7	29.2
25	Shale	Weak, highly weathered	11.4	84	100	3.2	1,676	20.2	31.5	2.4	31.2	0.8	38.4
26	Shale	Dark gray, hard with calcite	50.0	50	100	17.2	1,981	96.5	2.8	13.5	2.8	3.2	47.7
27	Shale	Dark gray, weathered, medium	9.3	60	100	14.5	1,981	54.5	6.6	16.1	15.6	1.2	37.2
28	Shale	Weathered	12.4	70	90	3.0	1,219	9.1	17.0	15.2	17.0	0.7	47.2
29	Shale	Hard	19.7	100	100	6.6	1,219	19.5	9.1	44.6	8.6	1.3	31.9
30	Shale	Hard, massive	44.8	80	100	5.0	1,524	8.0	5.6	1.9	1.8	1.4	26.0
31	Shale	Reddish brown	41.4	66	95	4.2	1,067	8.5	1.2	2.1	1.1	1.0	31.9
32	Shale	Brown	41.4	75	100	5.8	2,591	41.4	50.9	31.6	50.8	1.2	39.6
33	Shale	Brown	41.4	70	100	8.7	2,286	27.2	12.3	16.8	12.1	0.9	31.3
34	Shale	Brown	41.4	70	100	4.9	1,676	18.7	5.9	12.3	5.3	1.3	32.0

TABLE 1 (continued).

Test No.	Type of Rock	Rock Visual Description	Rock Properties			Socket Length (m)	Pile Diameter (mm)	O-Cell Applied Load (MN)	O-Cell Movements (mm)		Unit Side Shear		Concrete Strength, $f_c$ (MPa)
			$q_u$ (MPa)	RQD (%)	REC (%)				Upward	Downward	$z$ (mm)	$f_s$ (MPa)	
35	Shale	Soft to medium hard, closely fractured, weathered	33.1	95	100	9.4	1,829	27.5	3.0	25.4	3.0	0.9	24.6
36	Shale	Soft to medium hard, closely fractured, weathered	33.1	95	100	8.4	1,219	3.7	0.2	1.9	0.2	0.3	40.3
37	Shale	Reddish brown	32.1	66	100	4.8	2,591	15.7	73.4	22.7	73.4	0.7	24.7
38	Shale	Reddish brown	32.1	66	100	3.2	2,591	10.7	41.2	6.2	41.2	0.5	43.5
39	Shale	Red, poorly indurated	46.2	52	80	17.4	1,829	14.7	0.2	75.2	0.2	0.7	39.8
40	Shale	Trace white quartz	45.9	44	50	3.1	1,067	8.1	8.1	10.2	8.1	1.3	31.0
41	Shale	Gray, hard	45.5	65	95	6.2	1,372	13.3	0.9	0.5	0.8	1.1	27.6
42	Shale	Medium hard to hard	36.2	78	100	3.2	1,219	13.1	9.9	7.2	9.6	0.4	21.0
43	Shale	Medium hard	35.9	60	100	3.3	1,067	10.0	0.9	2.4	0.7	0.9	32.0
44	Shale	Black thin bedded	47.2	80	100	3.2	914	19.0	5.6	7.6	5.6	2.4	28.7
45	Shale	Hard with interbedded siltstone	46.5	90	98	2.9	914	11.5	23.4	8.0	23.4	2.4	31.9
46	Sandstone	Very hard	113.8	50	50	5.7	2,286	83.2	3.3	4.3	3.1	3.2	43.0
47	Sandstone	Reddish brown	43.1	90	97	5.2	2,438	35.2	6.5	10.8	5.5	1.5	31.0
48	Sandstone	Hard, slightly to extremely fractured	50.0	97	100	5.0	1,067	10.9	10.2	5.6	10.2	1.0	29.2
49	Sandstone	Weathered	6.2	27	76	12.6	1,524	26.1	36.6	12.5	11.4	1.6	29.3

50	Sandstone	Medium hard to hard	52.0	34	100	3.9	914	10.7	17.8	11.0	17.4	1.7	29.4
51	Sandstone	Medium hard	49.6	90	100	3.7	1,219	13.4	38.3	3.7	38.1	3.3	44.3
52	Sandstone	Hard	74.8	80	100	3.6	1,219	33.4	11.6	5.4	10.2	4.3	30.2
53	Mudstone	Medium hard	54.1	100	100	3.4	1,067	28.0	23.3	11.2	22.0	3.0	27.4
54	Mudstone	Weak	29.3	79	87	2.6	1,067	10.7	32.9	54.4	5.1	1.1	30.8
55	Siltstone	Sound	60.3	84	100	7.0	1,372	38.4	7.8	11.6	7.4	2.0	22.5
56	Siltstone	Gray to dark gray, gypsum inclusions	48.5	92	100	10.7	1,219	17.2	1.4	38.1	1.3	1.1	26.9
57	Siltstone	Hard, massive	42.2	61	100	5.5	1,829	11.3	15.4	3.9	15.0	1.3	29.9
58	Siltstone	Hard	34.5	20	100	10.4	1,829	20.5	2.3	56.5	2.0	0.8	30.2
59	Siltstone	Medium hard to hard	59.0	67	100	4.3	1,219	10.0	2.2	110.0	2.2	1.1	42.3
60	Claystone	Weathered	28.6	90	100	4.3	1,219	6.8	39.5	16.3	39.4	0.9	24.3
61	Limestone	Hard	59.3	95	100	6.2	762	4.7	1.0	1.7	1.0	0.5	44.1
62	Limestone	Hard	76.2	96	100	19.4	2,591	106.6	2.9	28.8	2.3	2.3	41.4
63	Limestone	Slightly fractured	74.8	93	100	4.2	1,829	23.7	2.0	2.6	2.0	2.4	34.5
64	Limestone	Slightly fractured	76.0	94	100	3.0	1,219	17.5	2.5	3.7	2.4	2.3	29.2
65	Limestone	Hard	33.5	90	100	2.5	1,829	39.2	2.9	4.6	2.5	1.7	29.9
66	Limestone	With shale seams	24.3	93	100	4.5	1,676	40.3	8.9	2.2	8.9	3.0	26.2
67	Limestone	Light to medium gray	30.5	100	100	8.7	1,219	40.6	3.0	3.0	1.8	2.8	42.3

TABLE 1 (continued).

Test No.	Type of Rock	Rock Visual Description	Rock Properties			Socket Length (m)	Pile Diameter (mm)	O-Cell Applied Load (MN)	O-Cell Movements (mm)		Unit Side Shear		Concrete Strength, $f_c$ (MPa)
			$q_u$ (MPa)	RQD (%)	REC (%)				Upward	Downward	$z$ (mm)	$f_s$ (MPa)	
68	Limestone	Gray to white, stylolite seams	34.5	65	100	4.0	1,676	10.0	7.7	24.1	7.6	1.1	33.0
69	Limestone	Whitish brown, close to moderately close spacing	31.3	78	100	0.5	711	6.7	21.8	3.7	21.8	2.4	36.3
70	Calcitic marble	Highly weathered	66.2	70	100	7.8	1,143	11.2	0.6	1.8	0.6	0.7	45.3
71	Calcitic marble	Highly weathered to weathered	66.2	70	100	6.7	1,143	11.2	1.4	1.4	1.4	1.2	54.5
72	Dolomite	Lightly weathered, white marble	69.8	83	95	6.5	1,676	27.4	3.1	1.0	3.1	1.8	27.8
73	Diabase	Hard, very closely jointed	108.9	95	100	3.1	1,676	11.3	0.6	0.3	0.6	0.9	39.6
74	Diabase	Hard, very closely jointed	108.9	95	100	2.6	838	6.3	0.3	0.4	0.3	1.2	35.0
75	Diabase	Weathered	104.8	98	100	6.4	1,676	17.7	0.5	91.6	0.5	0.9	44.8
76	Diabase	Very hard	104.5	95	100	7.3	2,591	59.1	2.5	4.2	2.3	0.9	46.2
77	Granite with quartz	Slightly fractured, slightly weathered	120.7	97	100	3.2	1,219	26.8	5.7	7.0	5.5	4.8	41.6
78	Granite	Weathered, moderately fractured	310.3	90	100	2.9	1,219	9.0	67.5	4.3	67.4	1.1	42.1

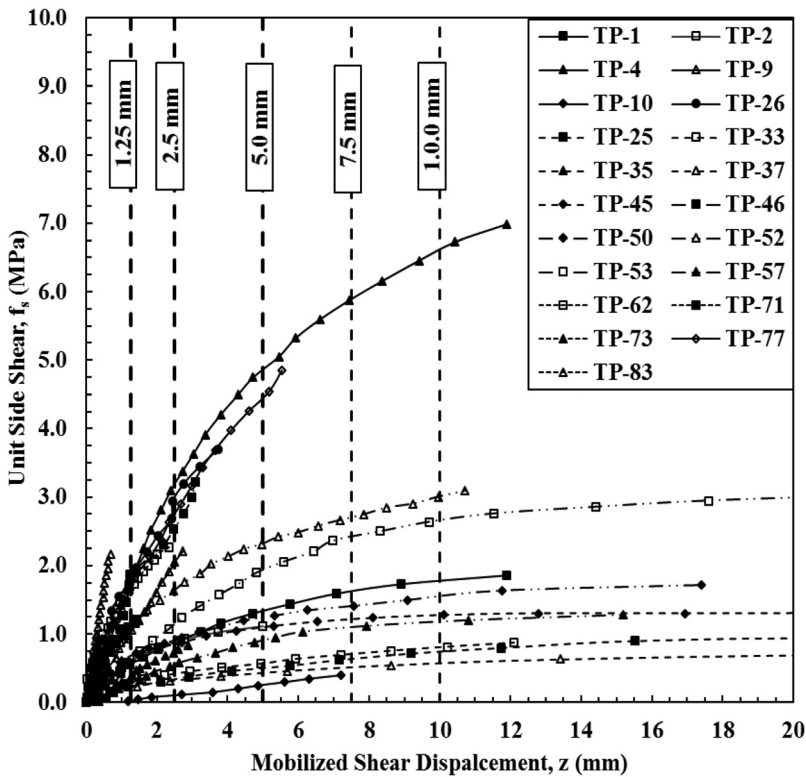
79	Basalt	Slightly weathered, moderately fractured	148.2	93	90	7.4	1,676	68.5	2.7	0.7	2.7	3.2	41.4
80	Dolerite	Gray, hard	120.7	100	100	3.7	1,676	31.9	1.0	5.7	0.7	2.3	37.5
81	Dolerite	Gray, hard	115.1	100	100	5.3	1,676	31.9	1.2	0.8	1.0	2.5	29.2
82	Dolerite	Gray, hard	172.4	100	100	5.2	1,676	27.8	1.4	2.1	0.9	2.0	35.9
83	Dolerite	Gray, hard	278.9	91	100	4.5	1,676	32.1	0.9	4.6	1.0	2.2	36.9
84	Tuff	Hard	24.1	100	100	14.6	1,499	47.0	2.8	1.8	2.8	2.0	74.5
85	Tuff	Hard	26.1	100	100	14.6	1,499	44.9	32.5	38.1	32.5	3.0	48.8
86	Tuff	Hard	11.1	100	100	14.6	1,999	65.0	21.1	58.4	21.1	1.8	45.0
87	Tuff	Highly to slightly weathered	15.2	96	95	19.0	1,199	17.1	1.5	2.0	1.3	1.7	45.8
88	Tuff	Highly to slightly weathered	15.2	96	95	19.0	1,199	15.3	1.3	1.8	1.3	1.8	58.8
89	Tuff	Hard	12.8	96	95	7.9	998	10.2	3.6	2.3	3.3	1.5	29.8

46 (52 %) have an RQD  $\geq 90$  %, with close to very close joints. The rock core recovery ratio (REC) varies in the range of 50 % to 100 %, with 84 rock formation sockets (94 %) having an REC  $\geq 90$  %. Overall, the data set primarily consists of sedimentary and metamorphic rock formation sockets with high REC and RQD values and a  $q_u > 25$  MPa.

### Identification of $f_{s,max}$ from $f_s$ versus $z$ Curve

The  $f_s$  versus  $z$  curves for 21 selected tests are plotted in Fig. 3. These 21 tests are selected such that they represent  $z$  varying from lower than 1.25 mm to higher than 25 mm. Of 21 selected tests, 12 are from sedimentary rock formations, 6 are from metamorphic rock formations, and 3 are from igneous rock formations. It can be observed that, of the 21 curves plotted in Fig. 3,  $f_s$  at  $z \geq 10$  mm is mobilized only in 10 curves (test piles 1, 4, 25, 33, 37, 45, 50, 52, 53, and 57), and the unit side shear curves become asymptotic at approximately 10 mm of shear displacement, implying that the maximum unit side shear seems to mobilize at around 10-mm shear

FIG. 3 Unit side shear curves ( $f_s$  vs.  $z$ ) for 21 selected bidirectional load tests.



displacement. In addition, based on the maximum applied test load for sockets with  $z > 10$  mm, the average additional capacity beyond 10-mm displacement is less than 5 % of the total capacity. Hence, 10-mm shear displacement, although an arbitrary value, can be considered a convenient upper bound for  $f_s$ , i.e.,  $f_{s,max} \approx f_{s,z=10\text{ mm}}$ .

From the total test data base, it can be observed that  $f_s$  at  $z \geq 10$  mm is mobilized in only 24 tests, of which 17 are in sedimentary rock formations, 4 are in metamorphic rock formations, and 3 are in igneous rock formations. Although there is only one curve in Fig. 3 with  $z \geq 10$  mm in an igneous rock formation, for the purpose of this analysis it is assumed that the previously mentioned convenient upper bound for  $f_s$ , i.e.,  $f_{s,max} \approx f_{s,z=10\text{ mm}}$  is also applicable to igneous rock formations. Thus, for any rock socket load test with its maximum mobilized  $z < 10$  mm, the measured  $f_s$  value may be considered less than ultimate, and hence using this measured value would result in a possibly overly conservative pile design.

## Prediction of $f_{s,max}$ from the Measured $f_s$ versus $z$ Curve with $z < 10$ mm

For those tests with  $z < 10$  mm in Table 1,  $f_{s,max}$  may be predicted using either hyperbolic curve-fit extrapolation or statistical extrapolation. In soils and rocks, the shape of the unit shear curves may be approximated by a hyperbolic function [10]. It is often possible to extrapolate an  $f_s$  versus  $z$  curve to  $f_{s,max}$  by hyperbolic curve-fitting. However, the hyperbolic curve-fit extrapolation has its limitations. Among the 89 tests reported in Table 1, 52 mobilized only to a maximum value of  $z < 5$  mm, i.e., less than half of  $z$  at  $f_{s,max}$ . Of these 52 tests, 42 mobilized only to a maximum value of  $z \leq 2.5$  mm. To predict the  $f_s$  value at  $z = 10$  mm (i.e.,  $f_{s,max}$ ) for tests with measured  $z < 5$  mm, hyperbolic extrapolation of an  $f_s$  versus  $z$  curve to a factor of 2 to 4 times the maximum measured  $z$  value may not be desirable and will very likely result in unreliable values. In addition, for tests with maximum measured  $z$  values  $\leq 1.25$  mm, which are still in a relatively linear range, hyperbolic extrapolation cannot be applied. Hence, the statistical extrapolation approach to predict  $f_{s,max}$ , as explained in the following section, is proposed as the preferred  $f_{s,max}$  prediction method.

### STATISTICAL EXTRAPOLATION TECHNIQUE

In the statistical extrapolation approach, for each  $f_s$  versus  $z$  curve in the data set, first the ratios of  $f_s$  at  $z = 2.5$  to 1.25 mm, 5.0 to 2.5 mm, 7.5 to 5.0 mm, and 10.0 to 7.5 mm are calculated (as applicable given their maximum mobilized  $z$  value). Second, the statistical distribution for each  $f_s$  ratio data set is analyzed along with its basic statistical parameters. Third, based on the statistical analysis, a representative value for each  $f_s$  ratio data set is derived. In Figs. 4–7, histograms for all four  $f_s$  ratio data sets are plotted along with their statistical parameters. Each  $f_s$  ratio data set has a minimum of 30 data points except the  $f_{s,z=10\text{ mm}}$  to  $f_{s,z=7.5\text{ mm}}$  ratio data set. The frequency distribution of each  $f_s$  ratio data set indicates normal distribution with median = mean. Thus, the average values of each  $f_s$  ratio data set can be

FIG. 4 Histogram for ratio of  $f_s$  at 2.5- to 1.25-mm shear displacements.

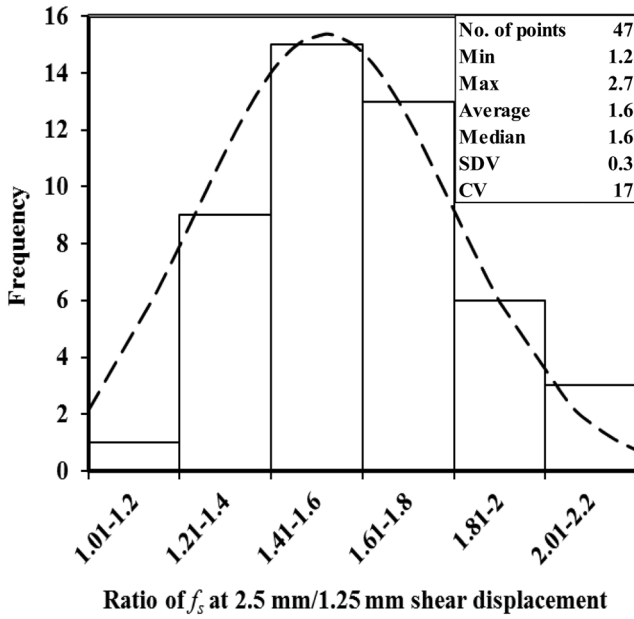
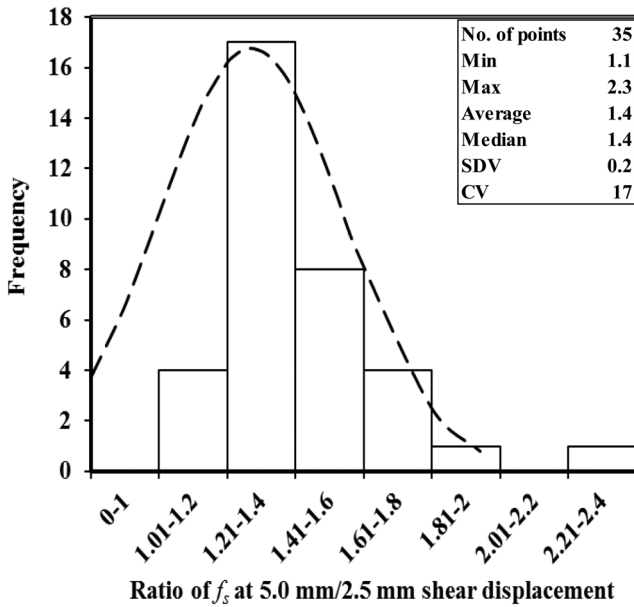
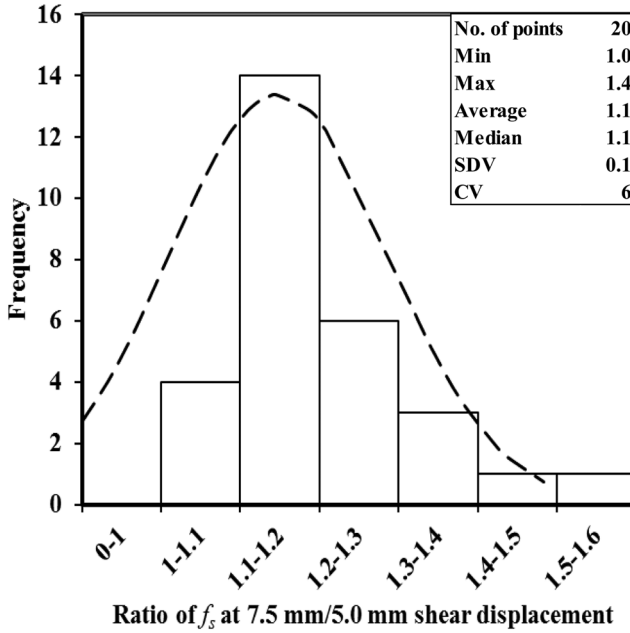


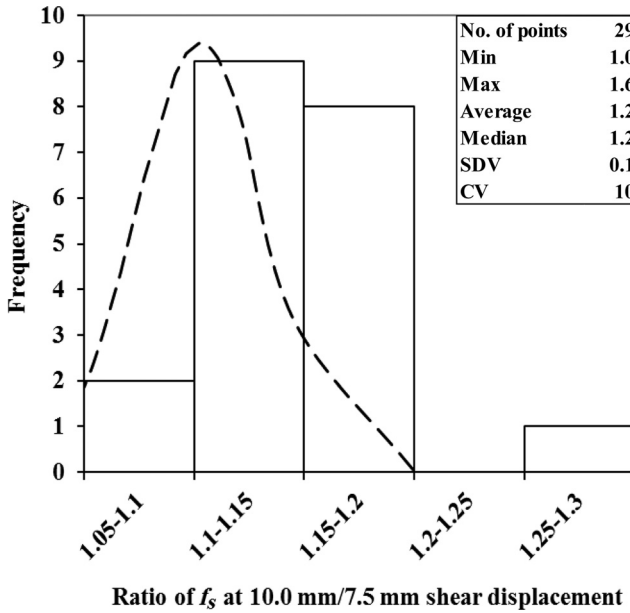
FIG. 5 Histogram for ratio of  $f_s$  at 5.0- to 2.5-mm shear displacements.



**FIG. 6** Histogram for ratio of  $f_s$  at 7.5- to 5.0-mm shear displacements.



**FIG. 7** Histogram for ratio of  $f_s$  at 10.0- to 7.5-mm shear displacements.



considered as its representative values and are presented in [Table 2](#). By considering  $f_{s,z = 1.25 \text{ mm}}$  as the basis value and using the  $f_s$  ratio representative values in [Table 2](#),  $f_s$  values at different  $z$  values, including  $f_{s,max}$ , can be predicted. By following this technique, for the tests that did not reach  $f_{s,max}$ ,  $f_s$  versus  $z$  curves can be developed up to  $f_{s,z = 10 \text{ mm}}$ .

### VALIDATION OF STATISTICAL PREDICTION TECHNIQUE

The proposed statistical prediction technique is validated by comparing measured and predicted  $f_s$  versus  $z$  curves and measured and predicted  $f_s$  values at  $z = 2.5, 5.0, 7.5,$  and  $10.0 \text{ mm}$ , as applicable for each test in the database. In the first method, both measured and statistically predicted  $f_s$  versus  $z$  curves for six tests are compared ([Fig. 8](#)). These six tests are selected because their measured  $z$  value is greater than  $10 \text{ mm}$ ; hence, the predicted values can be compared up to  $f_{s,max}$ . To develop the predicted curve,  $f_{s,z = 1.25 \text{ mm}}$  is taken as the base value, and then the remaining curve points are estimated using the  $f_s$  ratio values presented in [Table 2](#). In [Fig. 8](#), statistically predicted (dotted) curves match relatively well with measured (solid) curves in all tests except for the TP-4 curve. In the TP-4 curve, the predicted  $f_{s,max}$  value is 14 % lower (i.e., conservative) than the actual value. Overall, this comparison reasonably validates the statistical prediction technique. However, this method compared only those tests that have mobilized to  $z \geq 10 \text{ mm}$ .

To validate the statistical prediction technique further, the following second method is adopted: measured  $f_s$  values at  $z = 2.5, 5.0, 7.5,$  and  $10 \text{ mm}$  are plotted against predicted  $f_s$  values (see [Figs. 9–12](#), respectively). In this method,  $f_{s,z = 1.25 \text{ mm}}$  is also taken as the basis for estimating  $f_s$  at  $z = 2.5, 5.0, 7.5,$  and  $10.0 \text{ mm}$  using the  $f_s$  ratio values in [Table 2](#). For each plot, the average trend line along with its equation is plotted and compared to the  $y = x$  (dotted) line. In [Figs. 9–12](#), the slope of each average trend line is nearly equal to 1, indicating that the statistically predicted  $f_s$  values are close to the measured  $f_s$  values at their respective displacements, and the overall results validate the statistical prediction technique. Predicted  $f_s$  values are presented in [Table 3](#).

**TABLE 2**  $f_s$  ratio multiplication factors developed using statistical analysis.

$f_s$ Ratio with Reference to $z$ (mm)	Representative Value
$\frac{f_{s,z = 2.5 \text{ mm}}}{f_{s,z = 1.25 \text{ mm}}}$	1.6
$\frac{f_{s,z = 5.0 \text{ mm}}}{f_{s,z = 2.5 \text{ mm}}}$	1.4
$\frac{f_{s,z = 7.5 \text{ mm}}}{f_{s,z = 5.0 \text{ mm}}}$	1.2
$\frac{f_{s,z = 10 \text{ mm}}}{f_{s,z = 7.5 \text{ mm}}}$	1.1

FIG. 8 Comparison of actual and statistically estimated unit shear curves.

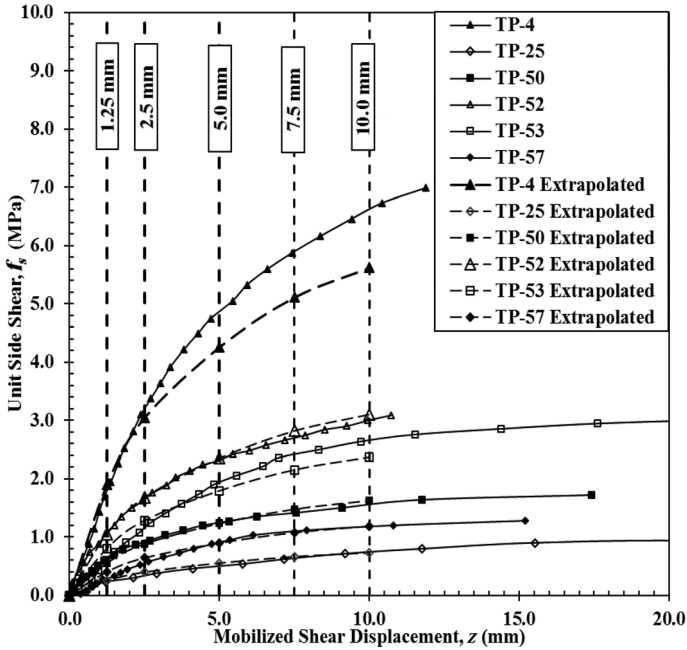


FIG. 9 Measured versus predicted  $f_s$  values at  $z = 2.5$  mm.

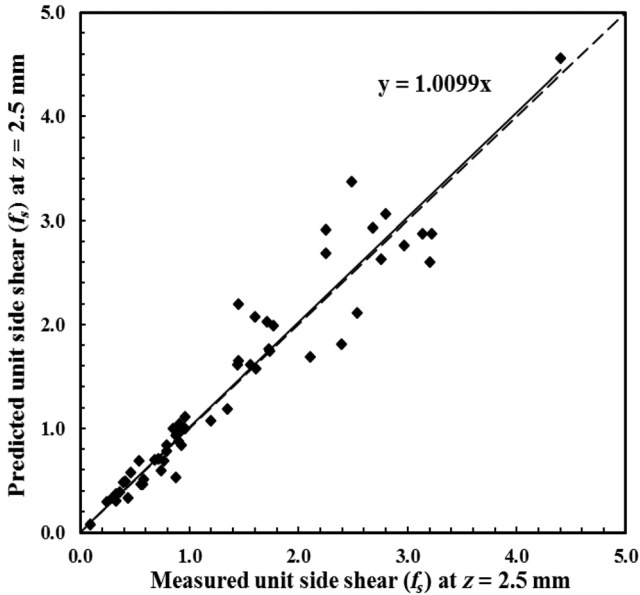


FIG. 10 Measured versus predicted  $f_s$  values at  $z = 5.0$  mm.

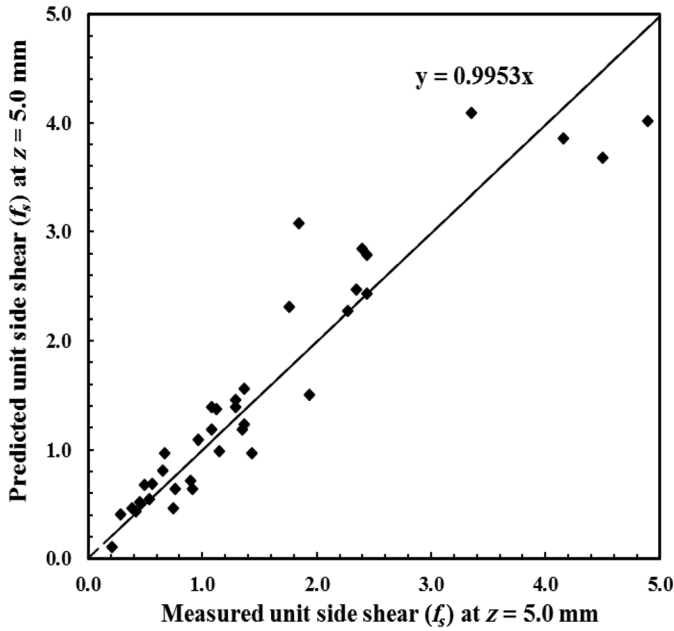


FIG. 11 Measured versus predicted  $f_s$  values at  $z = 7.5$  mm.

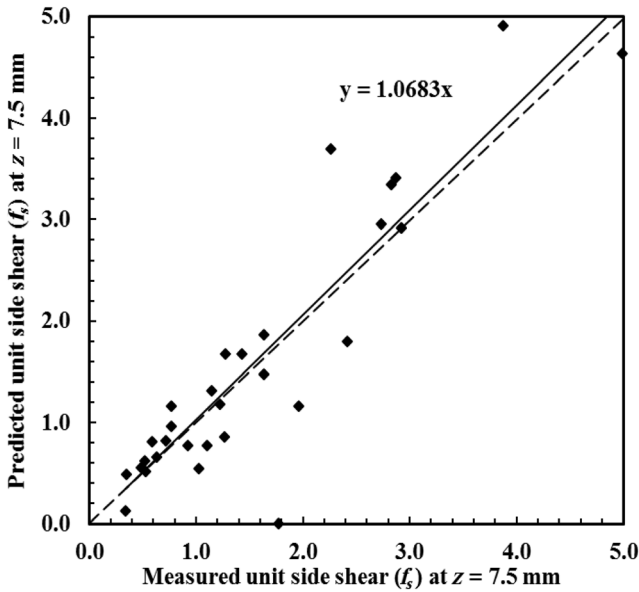


FIG. 12 Measured versus predicted  $f_s$  values at  $z = 10.0$  mm.

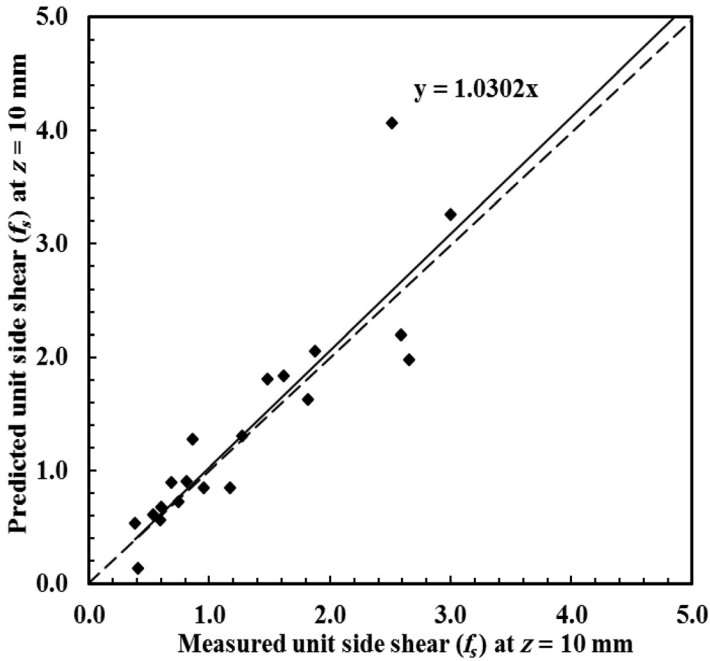


TABLE 3 Estimated or predicted unit side shear values for bidirectional test database.

Test No.	Type of Rock	Rock Strength, $q_u$ (MPa)	Unit Side Shear		$f_s$ at $z = 1.25$ (Mpa)	$f_s$ at $z = 2.5$ (Mpa)	$f_s$ at $z = 5.0$ (Mpa)	$f_s$ at $z = 7.5$ (Mpa)	$f_s$ at $z = 10$ (Mpa)	$f_s$ (AASHTO) (Mpa)
			$z$ (mm)	$f_s$ (MPa)						
1	Mica schist	33.1	11.9	1.9	0.6	0.9	1.4	1.6	1.8	1.2
2	Mica schist	32.4	5.0	1.1	0.6	0.9	1.1	1.3	1.5	1.2
3	Mica schist	32.8	4.0	2.0	0.7	1.4	2.0	2.4	2.6	1.2
4	Mica schist	53.1	11.9	7.0	1.8	3.2	4.9	5.9	6.7	1.5
5	Mica schist	51.7	5.1	6.2	2.8	4.4	6.2	7.4	8.2	1.5
6	Mica schist	59.3	1.4	1.1	0.9	1.5	2.1	2.5	2.8	1.6
7	Mica schist	44.8	14.7	1.8	1.3	1.6	1.7	1.8	1.9	1.4
8	Mica schist	44.1	14.7	4.2	1.8	2.7	3.4	3.9	4.3	1.4
9	Mica schist	55.2	2.7	2.2	1.1	2.1	2.9	3.5	3.9	1.5
10	Mica schist	32.8	3.3	0.8	0.4	0.7	1.0	1.2	1.3	1.2
11	Mica schist	30.3	0.6	0.6	1.1	1.8	2.5	3.0	3.3	1.0
12	Mica schist	30.3	0.5	0.7	1.3	2.1	2.9	3.5	3.9	1.1
13	Mica schist	45.2	0.6	0.7	1.2	1.9	2.6	3.1	3.4	1.3
14	Mica schist	45.2	0.7	0.8	1.2	1.9	2.7	3.2	3.6	1.3

TABLE 3 (continued).

Test No.	Type of Rock	Rock Strength, $q_u$ (MPa)	Unit Side Shear		$f_s$ at $z = 1.25$ (Mpa)	$f_s$ at $z = 2.5$ (Mpa)	$f_s$ at $z = 5.0$ (Mpa)	$f_s$ at $z = 7.5$ (Mpa)	$f_s$ at $z = 10$ (Mpa)	$f_s$ (AASHTO) (Mpa)
			$z$ (mm)	$f_s$ (MPa)						
15	Mica schist	45.2	0.5	0.9	1.7	2.8	3.9	4.7	5.2	1.0
16	Mica schist	45.2	0.1	0.8	1.2	1.9	2.6	3.2	3.5	1.4
17	Mica schist	45.2	0.4	0.9	1.2	1.9	2.6	3.2	3.5	1.3
18	Gneiss	54.2	1.3	0.8	0.8	1.2	1.7	2.0	2.2	1.1
19	Mica gneiss	112.8	2.3	0.7	0.7	1.1	1.6	1.9	2.1	2.2
20	Mica gneiss	112.8	2.4	0.9	0.6	0.9	1.2	1.5	1.6	2.2
21	Gneiss	113.8	1.1	3.0	3.0	4.9	4.9	5.9	6.4	2.2
22	Gneiss	88.0	0.3	1.0	1.0	1.5	2.1	2.6	2.8	1.9
23	Gneiss	88.0	0.4	1.1	1.1	1.7	2.4	2.9	3.2	1.9
24	Schist and gneiss	55.2	3.8	3.7	1.8	3.1	4.4	5.3	5.8	1.5
25	Shale	11.4	31.2	0.8	0.2	0.4	0.5	0.6	0.7	0.7
26	Shale	50.0	2.8	3.2	1.7	3.0	4.2	5.0	5.5	0.9
27	Shale	9.3	15.6	1.2	0.4	0.5	0.7	0.8	0.9	0.4
28	Shale	12.4	17.0	0.7	0.3	0.4	0.5	0.6	0.7	0.4
29	Shale	19.7	8.6	1.3	0.6	0.8	1.1	1.3	1.4	0.9
30	Shale	44.8	1.8	1.4	1.1	1.8	2.6	3.1	3.4	1.2
31	Shale	44.8	1.1	1.0	1.0	1.6	2.3	2.7	3.0	0.9
32	Shale	41.4	50.8	1.2	0.2	0.3	0.5	0.5	0.6	1.1
33	Shale	41.4	12.1	0.9	0.3	0.4	0.6	0.7	0.8	1.1
34	Shale	41.4	5.3	1.3	0.7	0.9	1.3	1.5	1.7	1.1
35	Shale	41.4	3.0	0.9	0.4	0.7	1.0	1.2	1.4	1.2
36	Shale	33.1	0.2	0.3	0.3	0.6	0.8	0.9	1.0	1.2
37	Shale	33.1	73.4	0.7	0.2	0.3	0.4	0.5	0.6	0.8
38	Shale	32.1	41.2	0.5	0.2	0.2	0.3	0.3	0.4	0.8
39	Shale	32.1	0.2	0.7	0.7	1.2	1.7	2.0	2.2	0.8
40	Shale	46.2	8.1	1.3	0.3	0.6	0.9	1.3	1.4	0.7
41	Shale	45.9	0.8	1.1	1.1	1.7	2.4	2.8	3.1	0.8
42	Shale	45.5	9.6	0.4	0.0	0.1	0.2	0.3	0.4	1.0
43	Shale	36.2	0.7	0.9	0.9	1.5	2.1	2.5	2.8	0.8
44	Shale	35.9	5.6	2.4	1.0	1.6	2.3	2.7	3.0	1.3
45	Shale	47.2	23.4	2.4	0.4	0.7	1.1	1.2	1.3	1.4
46	Sandstone	46.5	3.1	3.2	1.3	2.5	3.6	4.3	4.7	1.2
47	Sandstone	113.8	5.5	1.5	0.5	0.9	1.4	1.6	1.8	1.4
48	Sandstone	43.1	10.2	1.0	0.3	0.6	0.8	0.9	1.0	1.5
49	Sandstone	50.0	11.4	1.6	0.2	0.4	0.7	1.0	1.4	0.2
50	Sandstone	6.2	17.4	1.7	0.6	1.0	1.3	1.4	1.6	0.7
51	Sandstone	52.0	38.1	3.3	2.1	2.5	2.8	3.1	3.3	1.5
52	Sandstone	49.6	10.2	4.3	1.1	1.7	2.3	2.7	3.0	1.8
53	Mudstone	74.8	22.0	3.0	0.7	1.2	1.9	2.4	2.7	1.5

TABLE 3 (continued).

Test No.	Type of Rock	Rock Strength, $q_u$ (MPa)	Unit Side Shear		$f_s$ at $z = 1.25$ (Mpa)	$f_s$ at $z = 2.5$ (Mpa)	$f_s$ at $z = 5.0$ (Mpa)	$f_s$ at $z = 7.5$ (Mpa)	$f_s$ at $z = 10$ (Mpa)	$f_s$ (AASHTO) (Mpa)
			$z$ (mm)	$f_s$ (MPa)						
54	Mudstone	54.1	5.1	1.1	0.5	0.8	1.1	<i>1.3</i>	<i>1.4</i>	1.1
55	Siltstone	29.3	7.4	2.0	0.4	0.8	1.4	2.0	2.2	1.6
56	Siltstone	60.3	1.3	1.1	1.1	<i>1.7</i>	<i>2.4</i>	<i>2.9</i>	<i>3.2</i>	1.4
57	Siltstone	48.5	15.0	1.3	0.3	0.6	0.9	1.1	1.2	0.8
58	Siltstone	42.2	2.0	0.8	0.6	<i>0.9</i>	<i>1.3</i>	<i>1.5</i>	<i>1.7</i>	0.5
59	Sandy siltstone	34.5	2.2	1.1	0.8	<i>1.3</i>	<i>1.9</i>	<i>2.3</i>	2.5	1.1
60	Claystone	59.0	39.4	0.9	0.2	0.3	0.4	0.5	0.5	1.1
61	Limestone	59.3	1.0	0.5	0.5	0.9	<i>1.2</i>	<i>1.5</i>	<i>1.6</i>	1.6
62	Limestone	76.2	2.3	2.3	1.7	<i>2.3</i>	<i>3.2</i>	<i>3.8</i>	<i>4.2</i>	1.8
63	Limestone	74.8	2.0	2.4	1.1	<i>2.4</i>	<i>3.4</i>	<i>4.0</i>	<i>4.4</i>	1.8
64	Limestone	76.0	2.4	2.3	1.8	<i>2.3</i>	<i>3.2</i>	<i>3.8</i>	<i>4.2</i>	1.8
65	Limestone	33.5	2.5	1.7	1.3	1.7	<i>2.4</i>	<i>2.9</i>	<i>3.2</i>	1.2
66	Limestone	24.3	8.9	3.0	1.2	1.8	<i>2.4</i>	<i>2.8</i>	<i>3.1</i>	1.0
67	Limestone	30.5	1.8	2.8	1.9	2.8	<i>3.9</i>	<i>4.7</i>	<i>5.2</i>	1.1
68	Limestone	34.5	7.6	1.1	0.5	0.8	1.0	1.1	<i>1.3</i>	1.2
69	Limestone	31.3	21.8	2.4	0.7	1.0	1.4	1.6	1.9	1.2
70	Calcitic marble	66.2	0.6	0.7	<i>1.5</i>	<i>2.3</i>	<i>3.3</i>	<i>3.9</i>	<i>4.3</i>	1.3
71	Calcitic marble	66.2	1.4	1.2	1.1	<i>1.8</i>	2.5	3.0	3.3	1.3
72	Dolomite	69.8	3.1	1.8	1.0	1.6	<i>2.2</i>	<i>2.6</i>	<i>2.9</i>	1.6
73	Diabase	108.9	0.6	0.9	<i>1.8</i>	2.9	4.1	4.9	5.4	2.2
74	Diabase	108.9	0.3	1.2	<i>2.3</i>	<i>3.7</i>	<i>5.2</i>	<i>6.3</i>	<i>6.9</i>	2.2
75	Diabase	104.8	0.5	0.9	<i>1.8</i>	2.9	<i>4.0</i>	<i>4.8</i>	<i>5.3</i>	2.1
76	Diabase	104.5	2.3	0.9	0.3	0.9	<i>1.2</i>	<i>1.5</i>	<i>1.6</i>	2.1
77	Granite with quartz	120.7	5.5	4.8	1.6	2.8	4.5	<i>5.4</i>	5.9	2.3
78	Granite	310.3	67.4	1.1	0.4	0.5	0.7	0.8	0.8	3.6
79	Basalt	148.2	2.7	3.2	1.6	3.2	4.5	<i>5.4</i>	5.9	2.5
80	Dolerite	120.7	0.7	2.3	2.3	<i>3.7</i>	<i>5.9</i>	<i>7.1</i>	<i>7.8</i>	2.3
81	Dolerite	115.1	1.0	2.5	2.5	4.0	6.4	7.7	8.5	2.2
82	Dolerite	172.4	0.9	2.0	2.0	<i>3.2</i>	<i>5.2</i>	<i>6.2</i>	<i>6.8</i>	2.7
83	Dolerite	278.9	1.0	2.2	2.2	3.5	5.5	6.6	7.3	3.5
84	Tuff	24.1	2.8	2.0	1.0	1.6	<i>2.3</i>	<i>2.7</i>	<i>3.0</i>	1.0
85	Tuff	26.1	32.5	3.0	1.4	1.4	1.8	2.3	2.5	1.1
86	Tuff	11.1	21.1	1.8	1.0	1.4	1.8	1.8	1.8	0.7
87	Tuff	15.2	1.3	1.7	1.7	2.7	<i>3.7</i>	<i>4.5</i>	<i>4.9</i>	0.8
88	Tuff	15.2	1.3	1.8	1.8	2.9	<i>4.1</i>	<i>4.9</i>	<i>5.4</i>	0.8
89	Tuff	12.8	3.3	1.5	1.0	1.4	2.0	<i>2.4</i>	2.7	1.5

Note: Predicted  $f_s$  values are shown in italics.

## Empirical Relations for Estimating Unit Side Shear from Uniaxial Compressive Strength of Rock

Normalized  $q_u$  versus normalized  $f_{s,max}$  (i.e.,  $f_{s,z} = 10$  mm) values for all 89 tests (Table 1) are plotted in Fig. 13. This plot contains either measured or statistically predicted  $f_{s,z} = 10$  mm values. Statistically predicted  $f_s$  values are used only for those tests that have not mobilized to  $z \geq 10$  mm. An average trend line along with upper- and lower-bound lines are drawn along with corresponding Eqs 5–7.

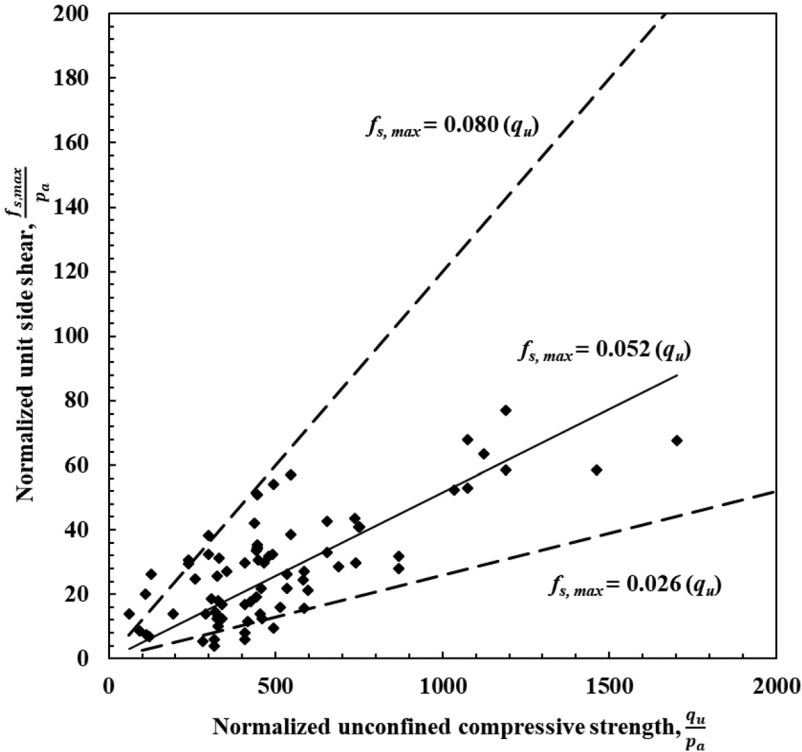
$$\text{Lower bound: } f_{s,max} = 0.026 q_u \quad (5)$$

$$\text{Average: } f_{s,max} = 0.052 q_u \quad (6)$$

$$\text{Upper bound: } f_{s,max} = 0.080 q_u \quad (7)$$

Eq 5 and Eq 7 represent lower- and upper-bound values, respectively, for 95 % of the total data points, whereas Eq 6 represents the average trend line. It is

FIG. 13 Normalized uniaxial strength versus normalized unit side shear at  $z = 10$  mm.



observed that as  $q_u$  increases, the spread in the  $f_s$  value also increases. This increase in spread can be attributed to various factors such as construction method, rock type, rock formation and its RQD, socket dimensions, etc. Quantification of the influence of these factors is beyond the scope of this paper.

#### VALIDATION OF EMPIRICAL RELATION BETWEEN $f_s$ AND $q_u$

Because Eq 6 is developed using both measured and predicted  $f_{s,z=10\text{ mm}}$  values, it can be validated by comparing the back-calculated equations to estimate  $f_s$  at  $z = 1.25, 2.5, 5.0,$  and  $7.5$  mm with empirical relations developed using measured data. Back-calculated equations are derived by applying the  $f_s$  ratio representative values (Table 2) to Eq 6 and are given as follows:

$$\text{For } z = 7.5 \text{ mm, } f_{s,z=7.5} = 0.047 q_u \quad (8)$$

$$\text{For } z = 5.0 \text{ mm, } f_{s,z=5.0} = 0.039 q_u \quad (9)$$

$$\text{For } z = 2.5 \text{ mm, } f_{s,z=2.5} = 0.028 q_u \quad (10)$$

$$\text{For } z = 1.25 \text{ mm, } f_{s,z=1.25} = 0.018 q_u \quad (11)$$

Normalized measured  $f_s$  and  $z$  values (non-italic  $f_s$  values in Table 3) for  $z = 1.2, 2.5, 5.0,$  and  $7.5$  mm are plotted in Figs. 14–17, respectively. The average trend lines along with their corresponding equation are also drawn in each plot and given below as well:

$$\text{For } z = 7.5 \text{ mm, } f_{s,z=7.5} = 0.041 q_u \quad (12)$$

$$\text{For } z = 5.0 \text{ mm, } f_{s,z=5.0} = 0.039 q_u \quad (13)$$

$$\text{For } z = 2.5 \text{ mm, } f_{s,z=2.5} = 0.028 q_u \quad (14)$$

$$\text{For } z = 1.25 \text{ mm, } f_{s,z=1.25} = 0.017 q_u \quad (15)$$

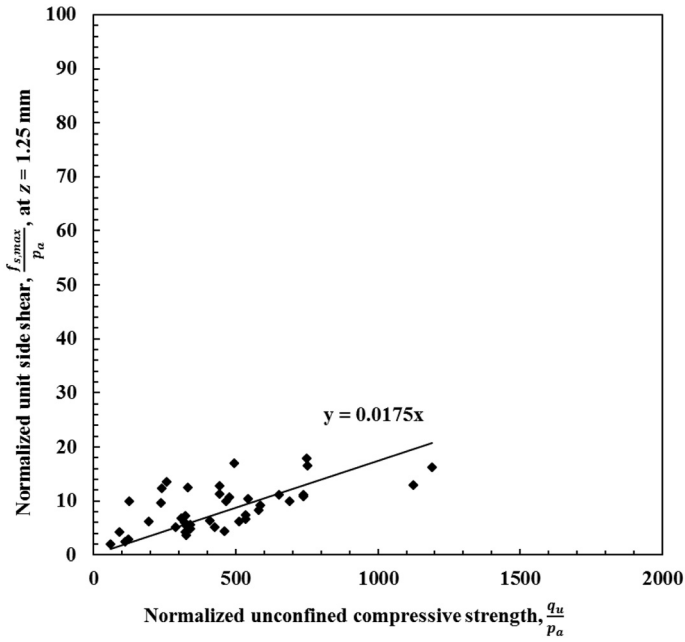
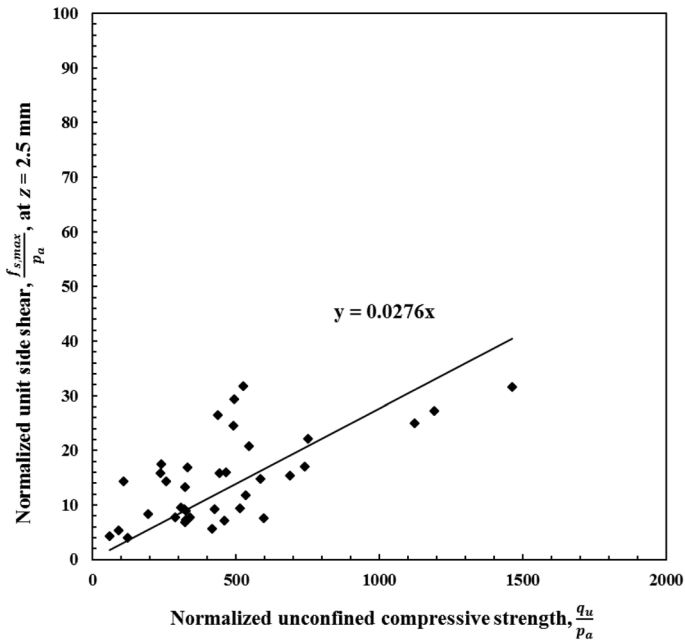
By comparing Eqs 12–15 with back-calculated Eqs 8–11, respectively, it is observed that the empirical relations developed using the measured  $f_s$  data are comparable to the back-calculated relations derived from Eq 6 and Table 2. The favorable comparison suggests Eq 6, which is based on measured and estimated  $f_s$  values, is valid for the displacements up to 10 mm.

#### EFFECT OF ROCK STRENGTH AND PILE DIMENSIONS ON UNIT SIDE SHEAR

To analyze the effect of magnitude of  $q_u$  on  $f_{s,max}$ , a proportional factor  $\psi$  is introduced and is defined as Eq 16:

$$\psi = \frac{f_{s,max}}{q_u} \quad (16)$$

Normalized  $q_u$  versus  $\psi$  for all the tests in Table 1 are plotted in Fig. 18. For tests that did not mobilize  $f_{s,max}$ , the statistically predicted  $f_s$  at  $z = 10$  mm was used to estimate  $\psi$ . From Fig. 18, it can be observed that the magnitude of  $\psi$  decreases as  $q_u$  increases. In other words, as  $q_u$  increases, the rate of increase in  $f_{s,max}$  decreases.

**FIG. 14** Normalized  $q_u$  versus normalized  $f_s$  values at  $z = 1.25$  mm.**FIG. 15** Normalized  $q_u$  versus normalized  $f_s$  values at  $z = 2.5$  mm.

**FIG. 16** Normalized  $q_u$  versus normalized  $f_s$  values at  $z = 5.0$  mm.

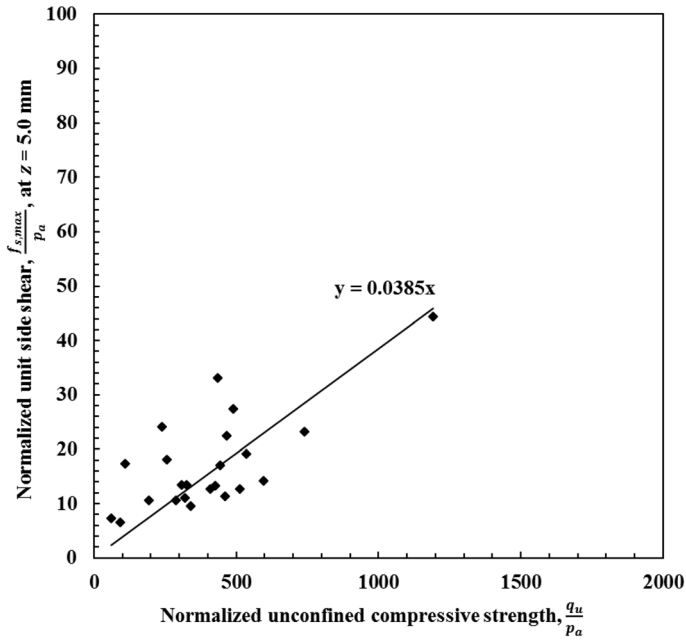


**FIG. 17** Normalized  $q_u$  versus normalized  $f_s$  values at  $z = 7.5$  mm.

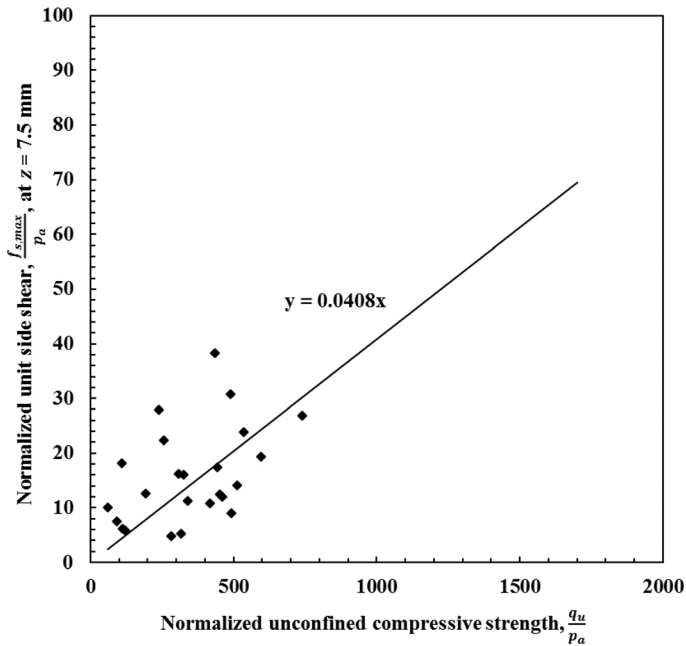
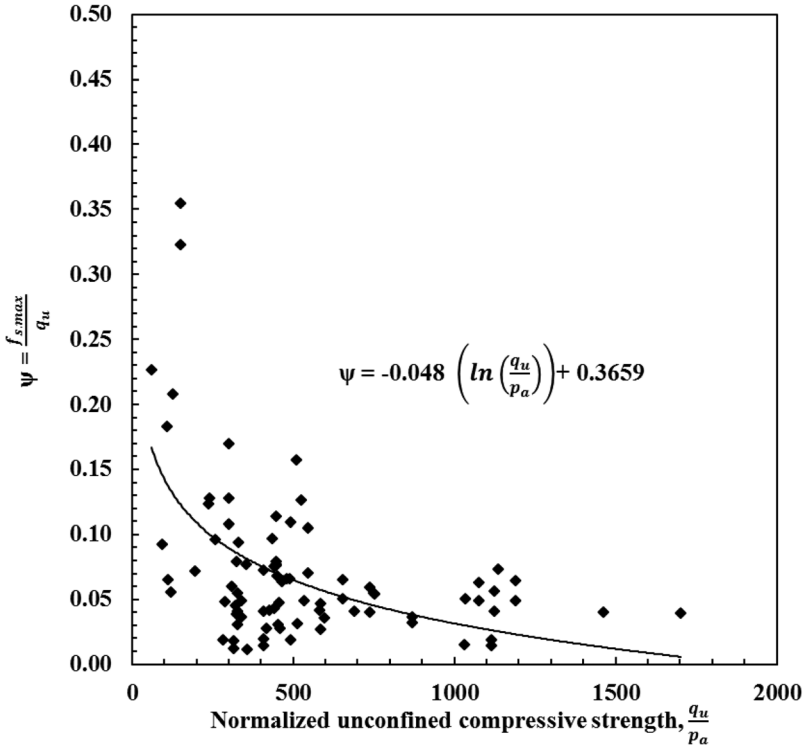


**FIG. 18** Influence of  $q_u$  on unit side shear  $f_{s,max}$ .



Kulhawy and Phoon [11] reported a similar relation for rock sockets. The relation between  $\psi$  and  $q_u$  can be approximated by Eq 17.

$$\psi = -0.048 \left( \ln \left( \frac{q_u}{p_a} \right) \right) + 0.3659 \tag{17}$$

To analyze the individual influence of socket length ( $L$ ), diameter ( $D$ ), and embedment ratio ( $\frac{L}{D}$ ) on  $f_{s,max}$ , ( $\frac{L}{D}$ ) versus  $\psi$ ,  $L$  versus  $\psi$ , and  $D$  versus  $\psi$  data points along with the correlation coefficient ( $r$ ) are plotted in Figs. 19–21, respectively. Based on the  $r$  value and an overall comparison, the data points in Fig. 19 and Fig. 20 indicate a proportional relation, whereas the data points in Fig. 21 indicate either no apparent relation or a weakly correlated inverse relation. Sinnreich [12] investigated the diameter scaling effect on  $f_s$  in the same rock type and concluded that for sockets in the same type of rock,  $f_s$  decreases with an increase in side shear. Among the three parameters, ( $\frac{L}{D}$ ),  $L$ , and  $D$ ,  $D$  appears to have the least influence on  $f_{s,max}$ . Data points in Fig. 19 have a better  $r$  value compared with Fig. 20, which indicates that the influence of ( $\frac{L}{D}$ ) on  $\psi$  is better quantifiable than  $L$  itself. In other

**FIG. 19** Influence of socket embedment ratio on  $f_{s,max}$ .

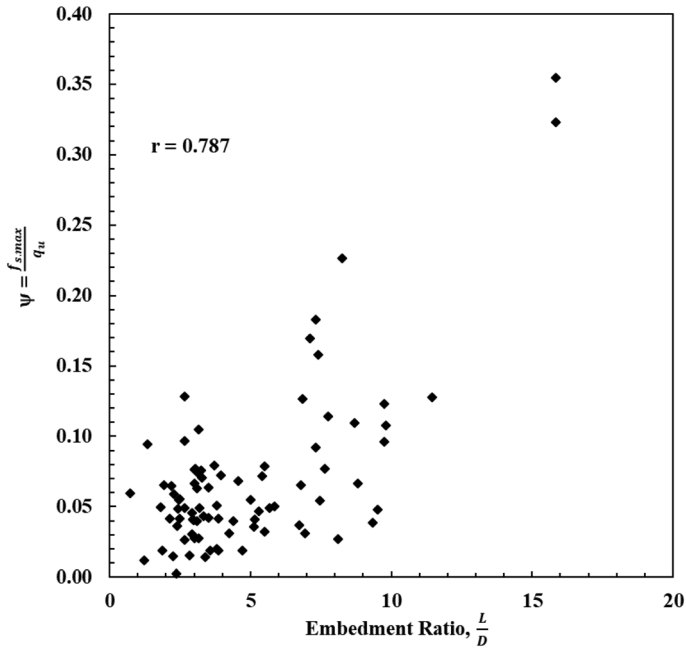


**FIG. 20** Influence of socket length on  $f_{s,max}$ .

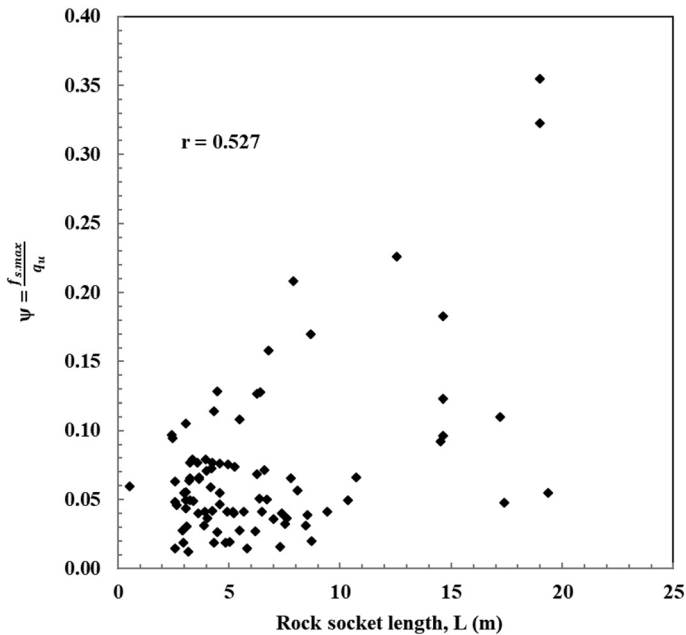
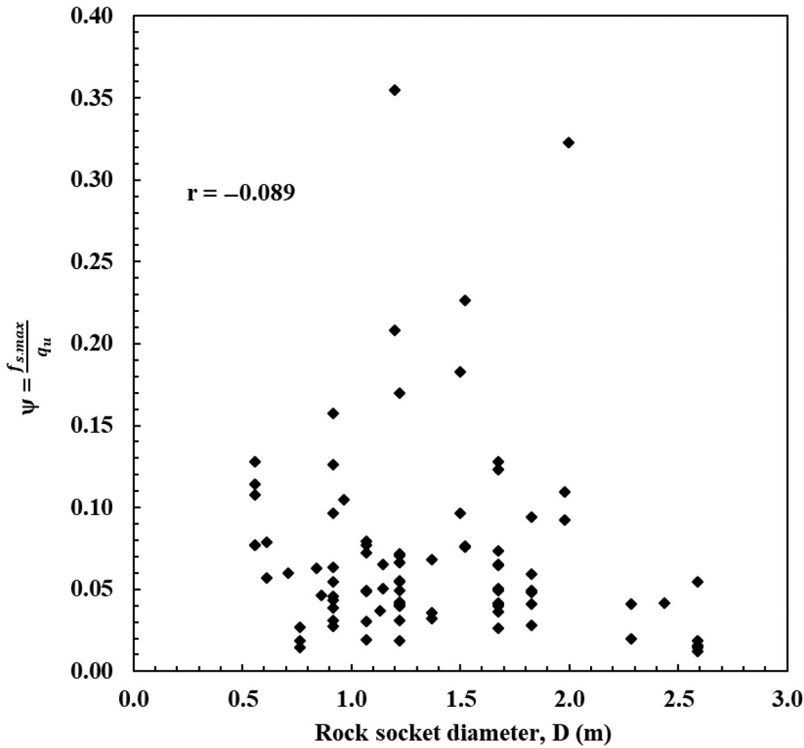


**FIG. 21** Influence of socket diameter on  $f_{s,max}$ .

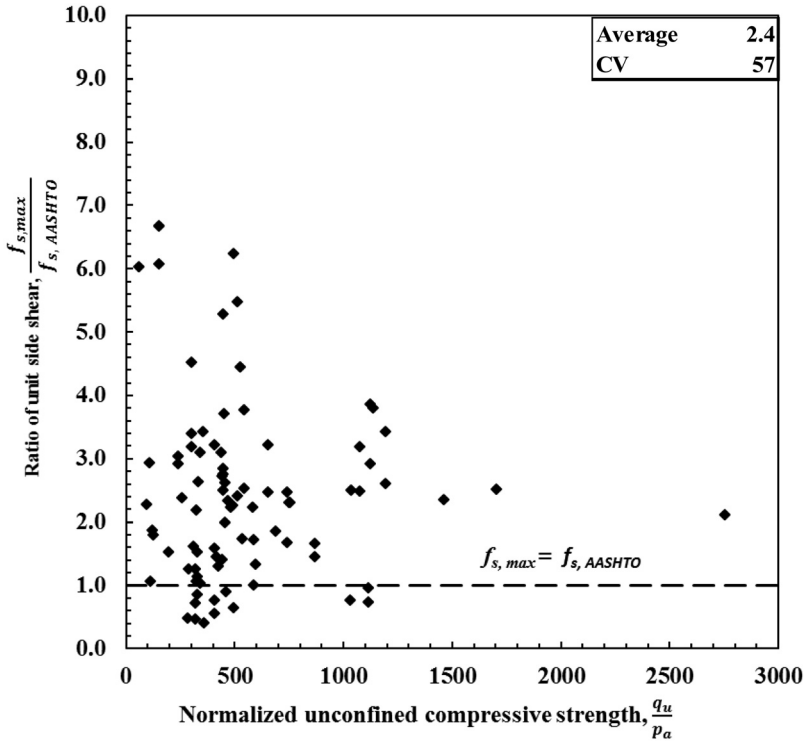


words, at a constant  $q_u$ ,  $f_{s,max}$  is more dependent on the socket embedment ratio than the socket length. To understand this behavior in detail requires further investigation into the mechanics of rock socket load transfer with respect to its length and diameter, which is beyond the scope of this paper.

#### COMPARISON WITH AASHTO $f_{s,max}$

$f_{s,max}$  values calculated using AASHTO's Eq 2 are presented in Table 3 for all 89 tests shown in Table 1. To calculate  $f_s$  (AASHTO),  $\alpha_E$  values for each rock socket are estimated using the RQD values in Table 1. As discussed earlier, Eq 2 limits the  $q_u$  value to  $f_c$ . However, in estimating the method's bias,  $q_u$  is not limited, and its measured value corresponding to the rock at each site is used to estimate  $f_{s,max}$  using AASHTO's Eq 2. The ratio of  $f_{s,max}$  (either measured or predicted) to  $f_s$  (AASHTO) for each test is calculated, and these ratio values are plotted in Fig. 22 against normalized  $q_u$  values on the x axis. The (dashed)  $f_{s,max} = f_s$  (AASHTO) line is also drawn. From Fig. 22, it can be observed that Eq 2 underestimates  $f_s$  for 79 of 89 tests. This clearly indicates that Eq 2 yields a conservative estimate, which can possibly result in longer socket lengths or diameters, or both.

**FIG. 22** Comparison of measured or predicted  $f_{s,max}$  with  $f_s$  (AASHTO) estimated from Eq 2.



## Discussion and Conclusions

The primary focus of this paper was to develop an empirical correlation between rock socket uniaxial compressive strength,  $q_u$  and ultimate unit side shear,  $f_{s,max}$ . Most of the rock-socketed bored pile load test data available in the literature do not reach ultimate capacity in side shear. As a result, a new relation for estimating  $f_{s,max}$  as a function of  $q_u$  using both measured and predicted  $f_{s,max}$  values from 89 bidirectional load tests on rock-socketed bored piles was developed. Based on the tests in which  $f_{s,max}$  was mobilized, it appears that  $f_{s,max}$  in rock sockets is typically mobilized at a shear displacement,  $z$ , of 10 mm. A statistical analysis of  $f_s$  ratios at displacement,  $z = 2.5$  to 1.25 mm, 5 to 2.5 mm, 7.5 to 5 mm, and 10 to 7.5 mm was performed to derive a representative value for each ratio, and these representative values can be used to predict  $f_s$  at different  $z$  displacements from a known measured  $f_s$  and corresponding  $z$  value. A simplified linear empirical relation for estimating  $f_{s,max}$  from rock  $q_u$  is proposed that indicates that approximately 5 % of  $q_u$  can be used as a predesign socket unit side shear resistance value when load test data are

not available. Analysis of socket length,  $L$ , diameter,  $D$ , and embedment ratio ( $\frac{L}{D}$ ) indicate that ( $\frac{L}{D}$ ) has the greatest influence on  $f_{s,max}$  whereas  $D$  does not have a significant influence.

Because  $f_s$  of a rock socket is significantly dependent on RQD, joint formations, and REC, the empirical relation (Eq 6) for  $f_s$  as function of  $q_u$  should be used with caution. The data set of 89 bidirectional load tests and corresponding  $q_u$  values is limited, with 70 % of the sockets with an RQD  $\geq 70$  and 90 % of the sockets with an RQD  $\geq 60$ . Based on the rock formation description and RQD for each socket of this paper's data set and recommendations of O'Neill and Reese [6] for  $\alpha_E$ , a conservative estimate of  $\alpha_E$  would be in the range of 0.8 to 1.0 for more than 90 % of the tests in the data set. By considering an average value of  $\alpha_E = 0.9$  and incorporating it into Eq 6 to account for RQD, Eq 6 would become Eq 18:

$$f_{s,max} = 0.058 (\alpha_E) (q_u) \quad (18)$$

However, in real field conditions, the process of rock classification and description is subjective and depends on the engineer or technician's experience with classification. Thus, Eq 6, which is developed from the entire database, could be considered better suitable for use in estimating socket predesign unit shear value.

Because the reported database has only three tests that mobilized  $f_{s,max}$  in igneous rock formations, it can be argued that the developed empirical equations and the conclusions are mostly applicable to sedimentary and metamorphic rock formations. In addition, because 90 % of the data set sockets have an RQD  $\geq 60$ , the data base can be statistically skewed. Hence, these empirical equations must be used with caution for rock formations with RQD values below 60 %.

## References

- [1] Kulhawy, F. H., Prakoso, W. A., and Akbas, S. O., "Evaluation of Capacity of Rock Foundation Sockets," *40th U.S. Rock Mechanics Symposium (Alaska Rocks 2005): Rock Mechanics for Energy, Mineral and Infrastructure Development in the Northern Regions*, American Rock Mechanics Association, Alexandria, VA, 2005, pp. 1-8.
- [2] O'Neill, M. W., "Side Resistance in Piles and Drilled Shafts," *J. Geotech. Eng.*, Vol. 127, No. 1, 2001, pp. 3-16.
- [3] Schmertmann, J. H. and Hayes, J. A., "The Osterberg Cell and Bored Pile Testing—A Symbiosis," *Proceedings of the Third International Geotechnical Engineering Conference*, Cairo University, Cairo, Egypt, 1997, pp. 139-166.
- [4] *AASHTO LRFD Bridge Design Specifications*, 7th ed., AASHTO, Washington, DC, 2014.
- [5] Horvath, R. G. and Kenny, T. C., "Shaft Resistance of Rock-Socketed Drilled Piers," *Symposium on Deep Foundations*, ASCE, New York, 1979, pp. 182-214.
- [6] O'Neill, M. W. and Reese, L. C., "Drilled Shafts Construction Procedure and Design Methods," Publication No. FHWA-IF-99-025, U.S. Department of Transportation, Washington, DC, 1999.
- [7] Osterberg, J. O., "What Has Been Learned about Drilled Shafts from the Osterberg Load Test," *Proceedings of the 24th Annual Members' Conference-DFI*, Deep Foundation Institute, Hawthorne, NJ, 1999, pp. 101-113.

- [8] Ayithi, A., Bullock, P. J., Khoo, H. S., and Ramana, G. V., "Technical and Economic Benefits of O-Cell Load Testing for Deep Foundations in India," presented at the *Indian Geotechnical Conference*, New Delhi, India, December 22–24, Indian Geotechnical Society, New Delhi, 2013, pp. 220–228.
- [9] Wood, W. R., Sinnreich, J., and Simmonds, A. J., "Use of Instrumented Static Load Tests on Deep Foundations for Optimization of Geotechnical Design," *Proceedings of the 9th International Symposium on Field Measurements in Geomechanics*, ACG, Perth, Australia, 2015, pp. 677–690.
- [10] Chin, F. K., "Estimation of the Ultimate Load of Piles from Tests Not Carried to Failure," *Proceedings of the 2nd Southeast Asian Conference on Soil Engineering*, University of Singapore, Singapore, 1970, pp. 81–92.
- [11] Kulhawy, F. H., and Phoon, K. K., "Drilled Shaft Side Resistance in Clay Soil to Rock," *Geotechnical Special Publication No. 38*, P. P. Nelson, T. D. Smith, and E. C. Cluke, Eds., ASCE, New York, 1993, pp. 172–183.
- [12] Sinnreich, J., "The Scaling Effect of Bored Pile Radius on Unit Shear Capacity," *Int. J. Geotech. Eng.*, Vol. 5, No. 4, 2011, pp. 463–467.